Exact solution of the 4-8/4/1 dimer model with OK multicritical point

1992 J. Phys. A: Math. Gen. 25 543

(http://iopscience.iop.org/0305-4470/25/3/014)

J. Phys. A: Math. Gen. 25 (1992) 543–559. Printed in the UK

Exact solution of the 4–8/4/1 dimer model with OK multicritical point

Carlos S O Yokoi† and John F Nagle‡

† Instituto de Física, Universidade de São Paulo, Caixa Postal 20516, São Paulo, Brazil
‡ Department of Physics, Carnegie Mellon University, Pittsburgh, PA 15213, USA

Received 7 August 1991

Abstract. A dimer model with competing interactions and ground state frustration is defined on the 4–8 lattice and the exact solution is obtained for the specific heat and densities of dimers. The model contains an energy parameter r, so phase transitions appear as lines in the (T, r) phase diagram. Two distinct kinds of striped incommensurate phase appear, separated from two commensurate and two disordered phases by a K-type transition line, and separated from each other by an O-type transition line. The phase diagram contains a novel OK multicritical point where a K-type transition line crosses an O-type transition line. The asymptotic scaling form at the OK multicritical point is the first member of a new class of scaling forms distinct from the two classes that encompassed all previous exact solutions of dimer models. The 4–8/4/1 model corresponds to the F-model at one temperature in a new kind of field.

1. Introduction

Exact and rigorous statistical mechanical solutions to specific models play a central role in the theory of phase transitions by providing data against which general theories are tested. Historically, the solution of the two-dimensional Ising model revealed that the variety of critical phenomena exceeds the limits prescribed by the classical theories. Exactly solved models even more artificial than the Ising model, such as the spherical model or the Gaussian model, have found enduring positions in the theory of phase transitions and critical phenomena. In this paper another datum is added to the still modestly small, but vigorously growing (Baxter 1982, Andrews *et al* 1984) set of exact solutions.

The starting point for the model (called the 4–8/4/1 model) solved in this paper resides in the field of adsorbed diatomic molecules on surfaces, otherwise known as dimer models. Such models have a number of other applications and they have enough history to have been the subject of a recent review (Nagle *et al* 1989). This might be considered to be an inauspicious starting point for new critical behaviour because all previous solutions of two-dimensional dimer models have yielded just two types of critical behaviour. The first O-type of transition is characterized by a symmetric logarithmic singularity in the specific heat, first obtained by Onsager (1944) for the two-dimensional Ising model. The second K-type of transition is characterized by a highly asymmetric transition with a square root divergence ($\alpha = \frac{1}{2}$) on one side only. This kind of transition, first obtained by Kasteleyn (1963) for a very simple dimer

0305-4470/92/030543+17$04.50

model on an anisotropic lattice, is closely related to striped commensurate-incommensurate, Pokrovsky-Talapov (1979) transitions.

Previous solved dimer models (Bhattacharjee 1984, Nagle and Yokoi 1987, Nagle *et al* 1989, Wu and Lin 1975) have exhibited both types of transitions as values of the model energy parameters are changed, with interesting crossover behaviour, but no model exhibited both types of transition as a function of temperature for a fixed value of the model parameters. The 4-8/4/1 model in this paper has this new property.

The 4-8/4/1 model will be explained in some detail in section 2 and the phase diagram will be derived in section 3. However, it is advantageous now to preview the phase diagram, shown in figure 1. The model has two energy intervals, ε and δ, to yield a one-parameter, $r=\delta/\varepsilon$, family. For $1<r<2$, the model undergoes, as T is increased from 0, a K-type transition from an anisotropic phase C1 to a striped incommensurate phase I1 followed by a reversed K-type transition to a disordered phase D1. For $2<r<r_{RE}=2.279\,898\ldots$ the model undergoes five transitions, including an extra pair of K-type transitions due to the re-entry of the C1 phase. What is new is the appearance of an O-type line of transitions for $r>2$. Although the appearance of O-type transitions and K-type transitions had not been unexpected, what *was* unexpected is the crossing of an O-line with a K-line, which occurs at $r_{OK}=3.296\,086\ldots$. This crossing will be called an OK multicritical point. It will be analysed in detail in section 5. As a result of the OK multicritical point, the sequence of thermal events for $r_{RE}<r<r_{OK}$ follows a substantially different course than for $r>r_{OK}$. For $r>r_{OK}$ there is a reversed K-type transition from the incommensurate I2 phase into the D2 disordered phase, which then undergoes a final O-type transition into the most disordered D1 phase. In contrast, for $r_{RE}<r<r_{OK}$ the final transition into the D1 phase is a reversed K-type transition and the O-type transition separates the incommensurate I2 phase from the incommensurate I1 phase. The distinction between the I1 and I2 phases will be completely characterized in section 4. In section 6 a correspondence between the dimer model and the F-model in a new kind of 4-sublattice or quarter field Q shows additional richness in the F-model. In turn, the correspondence identifies the O-line of transitions as the outgrowth of F-model criticality in zero staggered field S.

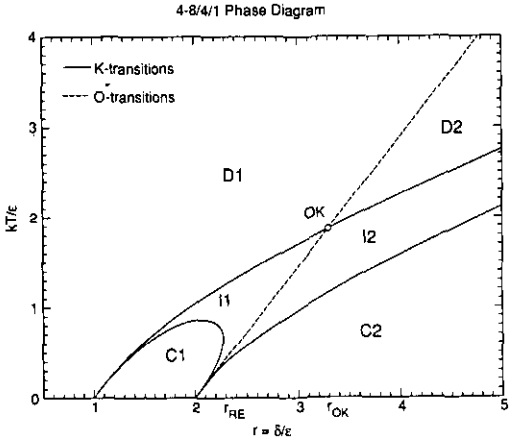

Figure 1. The phase diagram for the 4-8/4/1 dimer model. Transition temperatures are shown as a function of the ratio r of the two energies in the model.

2. 4-8/4/1 Model, ground states and basic excitations

Figure 2 shows the unit cell for the 4-8/4/1 model. The underlying lattice is the 4-8 lattice. Each allowed microstate of the model consists of dimers placed on the bonds of the lattice such that each vertex is covered by one and only one dimer. In addition, dimers on different bonds have different energies and activities. Each dimer on a bond labelled z in figure 2 has energy ε and activity $z=\exp(-\varepsilon/kT)$; each dimer on a bond labelled w has energy δ and activity $w=\exp(-\delta/kT)$; and each dimer on a bond labelled 1 has zero energy and activity 1. The 'Hamiltonian' for the model is given by its classical energy for each allowed microstate,

$$E = n_z\varepsilon + n_w\delta \tag{1}$$

where n_z and n_w are the numbers of dimers on z and w bonds, respectively. The partition function is

$$Z = \sum_{\text{microstates}} z^{n_z} w^{n_w}. \tag{2}$$

In this paper the energies ε and δ will be positive, so the model is frustrated in the sense that at most half the dimers in a microstate can have zero energy and at most half the low energy bonds may be occupied by dimers.

The 4-8/4/1 model has competing interactions as shown by the presence of three different kinds of ground states that appear as r is varied. Figure 3 shows the ground state for $r>2$; this ground state occurs at $T=0$ in the C2 phase in figure 1. One of the ground states that occurs at $T=0$ in the C1 phase in figure 1 ($2>r>1$) is shown in figure 4. The C1 ground states have a degeneracy factor $W=4$ for each unit cell; this comes about because the two dimers on each C and D square in figure 4 can be on either the vertical or the horizontal edges. The D1 phase ground states ($r<1$ in figure 1) are shown in figure 5; they carry a degeneracy factor $W=16$ for each unit cell. The $T=0$ boundaries of the D, C1 and C2 phases shown in figure 1 can be simply obtained by comparing the energies of the ground states. Also, the slopes of the phase lines at $T=0$ can be simply obtained by a Clausius-Clapeyron argument where $\Delta E = T\Delta S$ to first order in T. For example, for the D1 to C1 transition near $T=0$, one has $2(r-1)=(kT/\varepsilon)\ln 4$, so the slope of the phase line is $\mathrm{d}T/\mathrm{d}r=\varepsilon/(k\ln 2)$. These simple results provide checks on the exact calculation in the next section.

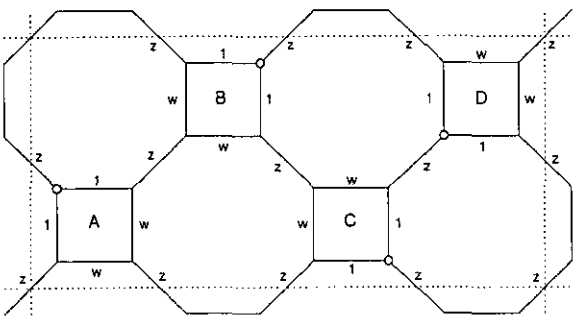

Figure 2. 4-8/4/1 model. The 4-8 lattice is shown by solid lines and the unit cell area is shown by dashed lines. Each bond is labelled with the activity, 1, z or w, of a dimer on that bond. For convenience in later figures, the corner of each square marked by an open circle identifies the vertex where the two bonds with activity 1 meet.

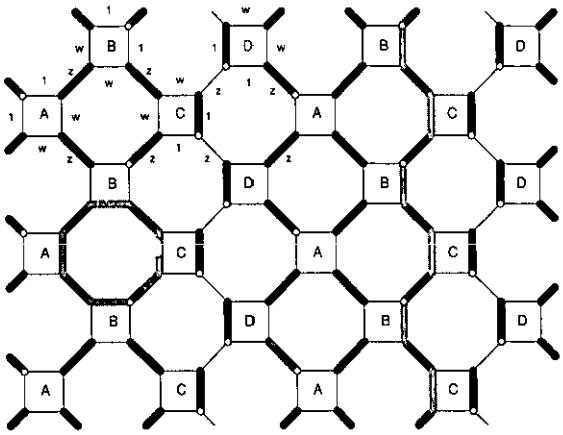

Figure 3. The unique C2 ground state for $r>2$ is shown by the solid black dimers located on some of the z and 1 bonds. This ground state energy is 6ε per unit cell. Perturbations are indicated by grey dimers that alternate with black ground state dimers. To effect the perturbation, those black dimers that alternate with the grey dimers are shifted to the grey positions. The perturbation on the left side of the figure is a localized perturbation around an elementary octagon with energy increase $3\delta-4\varepsilon$. The perturbation on the right side of the figure is a BC wall with energy increase $\delta-2\varepsilon$ per unit cell traversed.

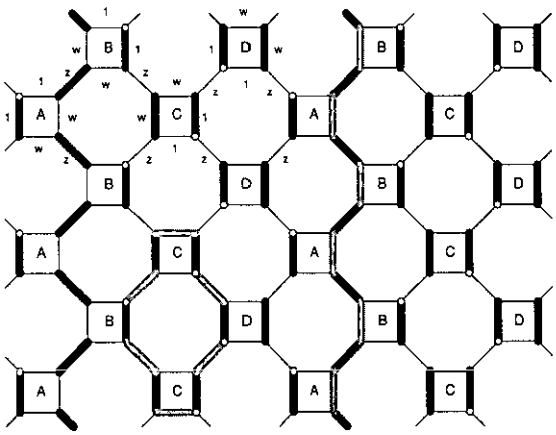

Figure 4. A C1 ground state for $1<r<2$ is shown by the solid black dimers. Per unit cell the ground state energy is $2\delta+2\varepsilon$ and the degeneracy is $W=4$. Perturbations are as described in figure 3. The local perturbation on the left increases E by 4ε and the AB wall on the right increases E by $2\delta-2\varepsilon$ per unit cell traversed.

Figures 3–5 also show some elementary perturbations from the ground states. These perturbations are conveniently classified as local perturbations and walls. The basic local perturbations consist of cyclic shifts of dimers around squares, as shown in figure 5, or around octagons, as shown in figures 3–5. By stringing together sequences of the basic local perturbations, larger perturbations can be made. The basic types of wall perturbations consist of AB walls, shown in figure 4, CD walls (not shown) or BC walls, shown in figure 3; DA walls are symmetrically equivalent to BC walls. Stringing local perturbations together with a wall may cause the wall to wander in the horizontal direction. The possibility of wandering walls suggests that a K-type transition from

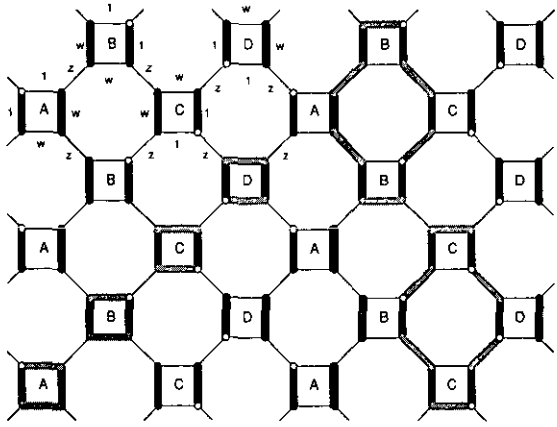

Figure 5. A D1 ground state for $r<1$ is shown by the solid black dimers. Per unit cell the ground state energy is 4δ and the degeneracy is $W=16$. Perturbations are as described in figure 3. The perturbations around the four squares, A, B, C and D on the left of the figure cost no energy and show the 16 fold degeneracy per unit cell in the ground state. The two local perturbations on the right around the two fundamental octagons increase E by $4\varepsilon-3\delta$ and $4\varepsilon-\delta$, respectively.

the anisotropic C1 and C2 phases into a striped incommensurate phase may take place as T is increased. Unlike the simple K-model of Kasteleyn (1963) the presence of local perturbations means that the model is not frozen into a simple ground state in the commensurate phases. This makes it much harder to predict the K-type transition temperature. It is therefore appropriate now to turn to the exact solution.

3. Exact solution

The Pfaffian method of obtaining exact solutions to two-dimensional dimer models has been amply reviewed (Montroll 1964, McCoy and Wu 1973, Nagle *et al* 1989). The solution takes the following form for the log of the partition function per unit cell:

$$f=\frac{1}{N}\ln Z=\frac{1}{8\pi^2}\int_0^{2\pi}\mathrm{d}\theta\int_0^{2\pi}\mathrm{d}\phi\,\ln\det\mathbf{M}(u,v,w,z) \tag{3}$$

where $\mathbf{M}$ is the 16×16 bond matrix of Kasteleyn (1963) and $u=\exp(\mathrm{i}\theta)$ and $v=\exp(\mathrm{i}\phi)$. We find $\det\mathbf{M}=|\det\mathbf{M}_1|^2$ where $\mathbf{M}_1$ is an 8×8 sub-block of $\mathbf{M}$ and

$$\det\mathbf{M}_1(u,v,w,z)=a_0-a_1v-a_{-1}v^{-1}+a_2(v^2+v^{-2}-u-u^{-1}) \tag{4}$$

where

$$a_0=z^8+4w^3z^4+4wz^4+16w^4$$

$$a_1=w^2z^6+z^6+8w^3z^2$$

$$a_{-1}=2wz^6+4w^4z^2+4w^2z^2$$

$$a_2=w^2z^4.$$

It is illuminating to highlight the locations of the zeros of det $\mathbf{M}_1(u, v, w, z)$ because these locations indicate the nature of the phases and their crossing of the unit circle in the complex v-plane locates the phase transition lines. Let us write

$$\det \mathbf{M}_1(v) = (v - v_1)(v - v_2)(v - v_3)(v - v_4)/v^2 \tag{5}$$

where

$$v_1 > v_2 > v_3 > v_4$$
$$v_i = v_i(\theta, w, z).$$

The interesting zeros are v_2 and v_3 which cross or touch the unit circle as a function of θ, w, z. Figure 6 shows the pattern of these two zeros in the different phases. The zero v_1 always lies outside the unit circle and v_4 lies inside the unit circle, so these are ignored in figure 6.

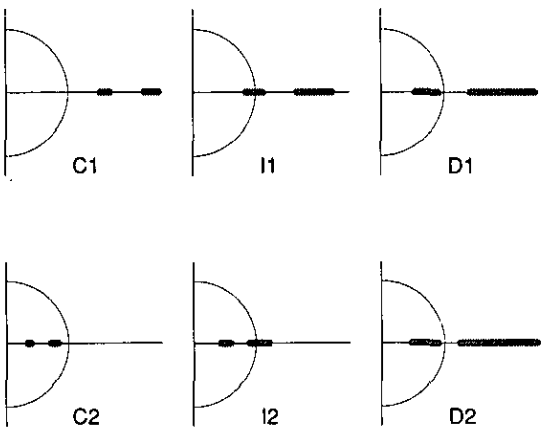

Figure 6. The pattern of zeros v_2 and v_3 of det $\mathbf{M}_1(\theta, v, w, z)$ in the complex v-plane for one value of (w, z) in each of the six phases. Each thick grey line shows the band for one of the zeros as θ is varied from 0 to π.

As usual (Nagle *et al* 1989), an O-type transition occurs when two bands of zeros simultaneously touch the same point on the unit circle for one value of θ. In the 4-8/4/1 model this occurs when

$$w = \frac{z^2}{2}. \tag{6}$$

A K-type transition occurs when the end of one band of zeros touches the unit circle for one value of θ. For the present model this occurs when

$$w = \frac{z(1-z)}{2-z}$$

or

$$w = \frac{z}{4(2-z)}[(z^4+4z^3-16z^2+8z+4)^{1/2}-(z^2-2z+2)] \tag{7}$$

or

$$w = \frac{z}{4(2+z)}[z^2+2z+2\pm(z^4-4z^3-16z^2-8z+4)^{1/2}].$$

The first relation in (7) gives the locus of the reverse K-type transition between phases I2 and D2 and between I1 and D1. The second relation in (7) gives the locus of the K-type transition from the C2 phase. The third relation in (7) gives the locus of the K-type transition from the C1 phase. As usual, a phase is a striped incommensurate phase if and only if a band of zeros crosses the unit circle as a function of θ. Figure 6 identifies the I1 and I2 phases as striped incommensurate phases for the 4-8/4/1 model.

The density of dimers of various types may be obtained by taking the appropriate derivative of $f = N^{-1} \ln Z$ in (3), such as

$$\rho_z = z\frac{\partial}{\partial z} f = 4 - \frac{1}{\pi}\int_0^{\pi} d\theta \sum_{|v_i|<1} \frac{z}{v_i}\frac{\partial v_i}{\partial z} \tag{8}$$

where the last equality results by performing the ϕ integration using residues. From the energy per unit cell $u = \varepsilon\rho_z + \delta\rho_w$, the specific heat per unit cell c can then be obtained by an additional derivative with respect to T, $c = du/dT$.

4. Thermodynamic functions

From the analysis in the preceding section we have calculated various thermodynamic functions which will be presented graphically in this section. Before presenting these results, however, a discussion will be given of a very useful density, called ρ_x, that was not obvious *a priori*.

The motivation for searching for a new density in addition to the obvious ones corresponding to density of dimers on z, w or 1 type bonds, is to find a density that varies only when the density of walls changes and not when local perturbations are activated. In the case of the 4-8/2/1 model solved earlier (Nagle and Yokoi 1987), this role was played by the linear combination $\rho_x = \rho_z - \rho_w$ which counted the density of light minus heavy walls. For the present 4-8/4/1 model there are also different kinds of walls, but all linear combinations of ρ_1, ρ_w and ρ_z are coupled to the local perturbations. A suitable ρ_x density was found by considering all possible perturbations to the activities (24 in number since the unit cell has 24 bonds). Many possibilities were eliminated by requiring changes in the density to be zero for local perturbations and non-zero for walls. The remaining possibilities all led to the same ρ_x. This ρ_x can be calculated by including perturbation activity factors x or x^{-1} to various bonds in the unit cell in figure 2. The factor x is attached to diagonal bonds running in the SE-NW direction and which cross either horizontal dashed unit cell line. The factor x^{-1} is attached to diagonal bonds running in the SW-NE direction and which cross either horizontal dashed unit cell line. It may be verified that any local perturbation does not change the power of x in the partition function, so it does not change ρ_x. The value of ρ_x for the D1 ground state is zero, for the C1 ground state it is $+1$, and for the C2 ground state it is -1. When an AB wall is introduced into the C1 ground state, it reduces the value of $N_h\rho_x$ by -1, where N_h is the number of unit cells in the horizontal direction in the entire lattice; if all AB walls are formed from the C1 ground state, one has the D1 ground state and $\rho_x = 0$. When either a BC or a DA wall is introduced into the C2 ground state, it increases the value of $N_h\rho_x$ by $+1$; if all BC and DA walls are formed from the C2 ground state, one has the C1 ground state. For this model CD walls always cost the highest free energy and do not play an active role.

The ρ_x density is one of the easiest thermodynamic functions to calculate because x is always paired with v in $\det \mathbf{M}_1(u, v, x, w, z)$. Therefore,

$$\rho_x = x(\partial f/\partial x)|_{x=1} = v(\partial f/\partial v)|_{x=1}$$
$$= \frac{\mathrm{i}}{2\pi^2}\int_0^{2\pi} \mathrm{d}\theta[\ln\det \mathbf{M}(\phi = 2\pi) - \ln\det \mathbf{M}(\phi = 0)]. \tag{9}$$

Since $[\ln\det \mathbf{M}(\phi = 2\pi) - \ln\det \mathbf{M}(\phi = 0)] = 2\pi i n(\theta, w, z)$ where $n(\theta, w, z)$ is the net number of times $\det \mathbf{M}(\phi, \theta, w, z)$ goes around the origin counterclockwise in the complex v-plane, n is the number of zeros of $\det \mathbf{M}$ minus the number of poles (including two from the v^{-2} factor in (5)) inside the unit circle. From figure 6 it can be seen that the number $n(\theta, w, z)$ only changes in the striped incommensurate phases I1 and I2.

Figures 7–12 show the results for the specific heat C and the densities ρ_x, ρ_w and ρ_z ($\rho_1 = 8 - \rho_w - \rho_z$), as a function of T for five different values of r. The specific heat in figure 7 is similar to the specific heat for the 4-8/2/1 model (Nagle and Yokoi 1987) with a K-transition followed by a reversed K-transition. For that 4-8/2/1 model the function ρ_{z-w} plays the same role as ρ_x in the present 4-8/4/1 model. However, ρ_x varies from 1 in the C1 phase to 0 in the D1 phase whereas ρ_{z-w} was 0 in both the low and high temperature phases for the 4-8/2/1 model. The specific heat in figure 8 has five singularities, although the amplitude of the O-type transition is very small compared with the amplitudes of the K-type transitions. The behaviour of ρ_x shows that there are three distinct non-incommensurate phases, C1, C2 and D1. Figure 9 shows the thermal behaviour for the re-entrant value r_{RE} where a K-type and a reverse K-type transition coalesce. The density functions exhibit discontinuous first derivatives, but the amplitudes conspire to yield a continuous specific heat C with discontinuous $\mathrm{d}C/\mathrm{d}T$. For larger r the O-type anomaly becomes more conspicuous as shown in figure 10 and the I1–D1 reverse K-type anomaly becomes weaker. Figure 11 suggests that

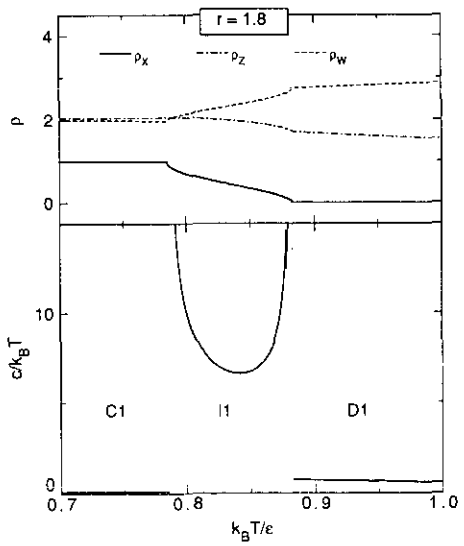

Figure 7. Results for the specific heat, c/k_BT, and the dimer densities, ρ_x, ρ_z, ρ_w as a function of temperature for $r = 1.8$.

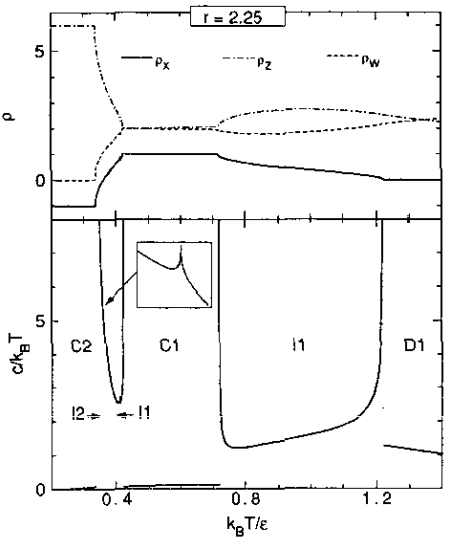

Figure 8. Results for the specific heat, c/k_BT, and the dimer densities, ρ_x, ρ_z, ρ_w as a function of temperature for $r = 2.25$.

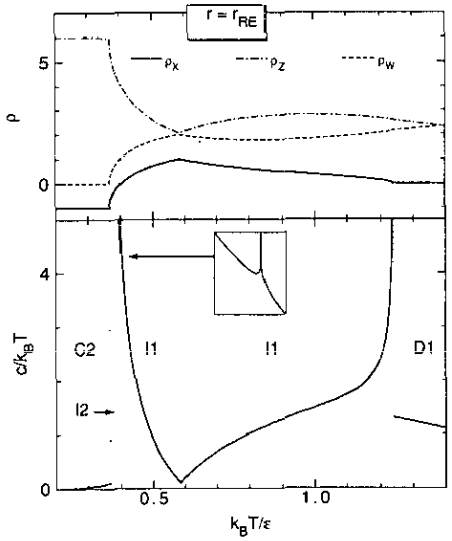

Figure 9. Results for the specific heat, c/k_BT, and the dimer densities, ρ_x, ρ_z, ρ_w as a function of temperature for $r = r_{RE} = 2.279\,848\ldots$.

the specific heat anomaly at the OK multicritical point is O-type and the reverse K-type anomaly has been suppressed, only to reappear again for $r > r_{OK}$ as shown in figure 12.

5. OK multicritical point

From the figures in the preceding section it appears that the specific heat anomaly near the multicritical point is symmetrical, similar to the specific heat of the O-type

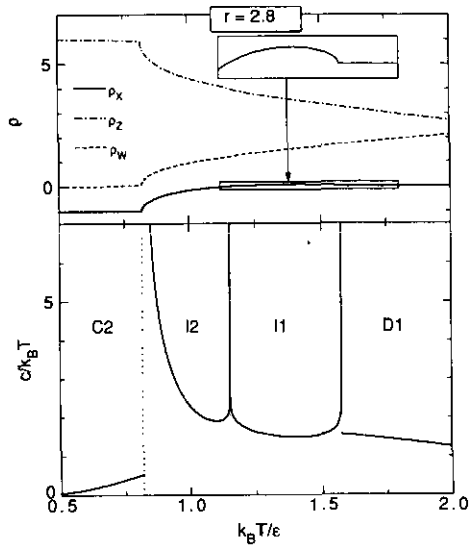

Figure 10. Results for the specific heat, c/k_BT, and the dimer densities, ρ_x, ρ_z, ρ_w as a function of temperature for $r = 2.8$.

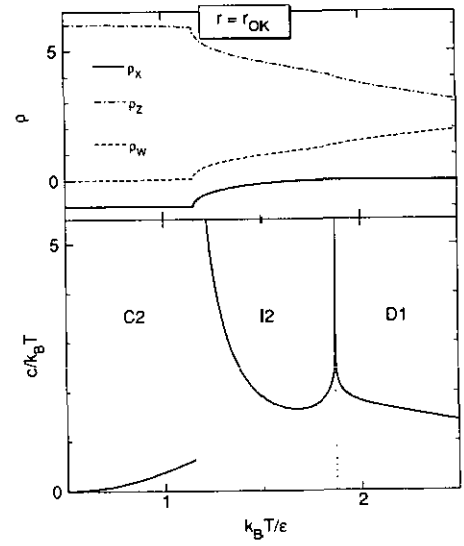

Figure 11. Results for the specific heat, c/k_BT, and the dimer densities, ρ_x, ρ_z, ρ_w as a function of temperature for $r = r_{OK} = 3.296\,086\ldots$.

transition and that the amplitudes of the K-type singularities may become vanishingly small. In this section an analysis will be performed to obtain the singular behaviour of the specific heat for $r = r_{OK}$, similar to the extraction of the specific heat singularities of the K-model and the SCD-model which were reviewed by Nagle *et al* (1989). This analysis is illuminating in its own right and is important to confirm the results of the numerical integrations that were required to obtain the graphs in the previous section.

It is appropriate to define two reduced temperatures; t_o will be the reduced temperature that goes to zero on the O-line of transitions and t_k will be the reduced

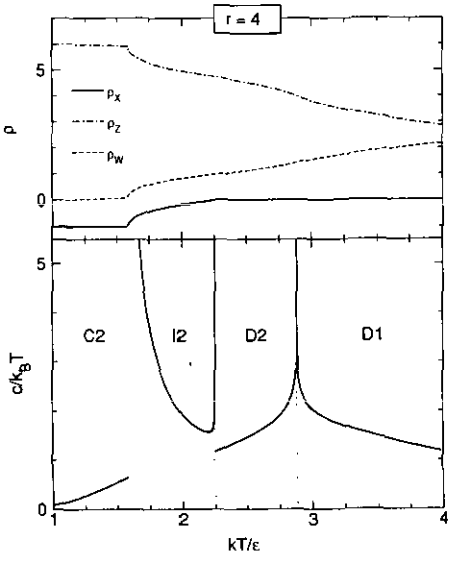

Figure 12. Results for the specific heat, c/k_BT, and the dimer densities, ρ_x, ρ_z, ρ_w as a function of temperature for $r = 4$.

temperature that goes to zero on the K-line of transitions that cross the O-line at the OK multicritical point. The singular contribution, f_s, comes from the small θ and ϕ region of the integral in (3),

$$f_s = \int_0^{\varepsilon} d\theta \int_0^{\varepsilon} d\phi \ln \det \mathbf{M}(z, w, \theta, \phi) \tag{10}$$

where ε is a small arbitrary cut-off, the sole effect of which is to ignore non-singular contributions to the free energy. Likewise, to determine the leading singular behaviour it is sufficient to consider only the most relevant terms in the function $\det \mathbf{M}(z, w, \theta, \phi)$, for small θ and ϕ. In the vicinity of the multicritical point the determinant is represented by the asymptotic form, omitting higher-order terms,

$$\det \mathbf{M} = (t_k t_o^2 + \theta^2 + \phi^2)^2 + (t_o \phi)^2. \tag{11}$$

When t_k remains non-zero, this form for $\det \mathbf{M}$ reduces to the O-type form,

$$\det \mathbf{M} = (t_o^2 + \theta^2 + \phi^2)^2. \tag{12}$$

When t_o remains non-zero, $\det \mathbf{M}$ reduces to the K-type form,

$$\det \mathbf{M} = (t_k + \theta^2)^2 + \phi^2. \tag{13}$$

As the multicritical point is approached for $r = r_{OK}$, $t_k \propto t_o = t$ and

$$\det \mathbf{M} = (t^3 + \theta^2 + \phi^2)^2 + t^2 \phi^2. \tag{14}$$

Details of the integration of (10) are given in the appendix. The results are, for $t_k > 0$,

$$f_s = -\frac{\pi}{2} t_o^2 (1 + 4t_k) \ln|t_o| \tag{15}$$

and for $t_k < 0$,

$$f_s = -\frac{\pi}{2} t_o^2 (1 + 4t_k) \ln|t_o| + 2\pi t_o^2 \sum_{n=1}^{\infty} 2^{2n} |t_k|^{(2n+1)/2} / (4n^2 - 1). \tag{16}$$

The multicritical scaling function in (15) and (16) contains the critical behaviour of the O-line as can be seen by taking $t_k \neq 0$ and $t_o \propto t$, obtaining both for $t_k > 0$ and $t_k < 0$

$$f_s \sim -t^2 \ln|t|. \tag{17}$$

The K-line behaviour is also contained in (15) and (16) as seen by taking $t_o \neq 0$ and $t_k \propto t$; there is no singular behaviour for $t > 0$ and for $t < 0$ the K-transition result

$$f_s \sim |t|^{3/2} \tag{18}$$

is recovered to lowest order. Finally, when the multicritical point is approached, $t_o \propto t$ and $t_k \propto t$. Then, for $t > 0$ (15) gives, to lowest order in t,

$$f_s \sim -t^2 \ln|t| \tag{19}$$

and for $t < 0$ (16) gives

$$f_s \sim -t^2 \ln|t| + |t|^{7/2}. \tag{20}$$

Therefore, the specific heat at the OK multicritical point is dominated by a logarithmic divergence, as suggested by numerical calculations, even though a weaker singular term $|t|^{7/2}$ is present in the free energy for $t < 0$.

It is interesting to consider the exact asymptotic scaling equation (15) and (16) in the context of general multicritical scaling. First, it is useful to rewrite det **M** in (14) as

$$\det \mathbf{M} = t^6[(1 + (\theta^2/t^3) + (\phi^2/t^3))^2 + (\phi^2/t^4)] \tag{21}$$

where the contributions for small θ come from the horizontal long wavelength wavenumbers and the contributions for small ϕ come from the vertical long wavelength wavenumbers. This strongly suggests that the horizontal θ correlations scale as $|t|^{-3/2}$, i.e. $\nu_x = \frac{3}{2}$, and that the vertical ϕ correlations scale as t^{-2}, i.e. $\nu_y = 2$. Although these values of ν have not been calculated rigorously for the OK multicritical point, the same analysis for the K-transition gives the values of $\nu_x = \frac{1}{2}$ and $\nu_y = 1$, and these were obtained rigorously (Yokoi *et al* 1986). Also, the same analysis gives the well-known values $\nu_x = 1 = \nu_y$ for the O-type transition. Since anisotropic hyperscaling, $2 - \alpha = \nu_x + \nu_y$, also holds for the K-type and O-type transitions, it is reasonable to consider its predicted value $\alpha = \frac{3}{2}$ for the OK multicritical point. This line of reasoning leads to the following OK multicritical scaling form

$$f_s \sim t_o^{2-\alpha} Y^{\pm}(t_k/t_o^{\phi}) \sim t_o^{7/2} Y^{\pm}(t_k/t_o) \tag{22}$$

where the value of the crossover exponent ϕ may usually be assumed to be one when critical lines cross at non-zero angle. Supposing the scaling function were $Y^-(x) = |x|^{3/2}$ and $Y^+ = 0$ in (22) very nicely reproduces (18) and the last term in (20). These are the terms that are associated with walls and with anisotropic correlation functions. However, to accommodate the O-type $t^2 \ln|t|$ singularity requires adding $|t_o|^{-3/2} \ln|t_o|$ to $Y^{\pm}$. This requires that the scaling function $Y^{\pm}(x, y)$ be a function of $y = t_o$ as well as of $x = t_k/t_o$. If the additional term did not dominate Y for $y \to 0$, then y would be *irrelevant* and we would have the usual scaling behaviour with the scaling function $Y(x, 0)$. However, the second term in $Y(x, y)$ evidently dominates for $y \to 0$, and the variable y cannot be ignored; it is in this respect a *dangerous irrelevant* variable (Fisher 1983).

The preceding discussion suggests that the correlation functions might be interesting at the OK multicritical point. The dominant $t^2 \ln|t|$ singular thermal behaviour would suggest $\nu = 1$ whereas the above scaling analysis of det **M** yields $\nu_x = \frac{3}{2}$ and $\nu_y = 2$.

Perhaps there are two different sets of relevant correlation lengths at the OK multicritical point, corresponding to choice of different dimer-dimer pair correlations in the unit cell. Perhaps one set of pair correlations has one of the sets of correlation lengths and exponents and another set of pair correlations has the other.

In summarizing this section it may be worthwhile to state how the OK multicritical point in this paper fits into the spectrum of multicritical points. Ordinary multicritical points may be characterized as having critical exponents that have values different from the critical exponents of the critical lines meeting at the multicritical point. A trivial multicritical point may be characterized by two critical lines crossing, as in this paper, but with the critical behaviour of neither line being affected by the crossing. The OK multicritical point is neither ordinary nor trivial. The critical behaviour at the OK point is dominated by the logarithmic singularity of the O-transition, so no new exponents appear, unlike ordinary multicritical points. However, near the OK point the K-transition is strongly damped by a factor of t_o^2, so one of the transitions is strongly affected by the crossing, unlike a trivial multicritical point.

Finally, it may be mentioned that the OK multicritical point is different from the multicritical point found by Nienhuis *et al* (1984) and again by Nagle and Yokoi (1987). That multicritical point, which is an O-transition when approached from certain directions, lies at the intersection of two K-transition lines. Also, the sequence of phases as one proceeds around the multicritical point is C-IC-C-IC, not the C-C-IC-IC sequence for the OK multicritical point studied here.

6. Correspondence with the F-model in a quarter field

Baxter (1970) used dimer models on the 4-8 lattice to solve the six-vertex F-model in a staggered field at one temperature. It is therefore appropriate to investigate what vertex model corresponds to the present 4-8/4/1 dimer model. This investigation is rewarding not only in illuminating additional richness in the F-model, but it also reveals the underlying dimer model phase diagrams in a more symmetrical fashion.

The basic correspondence between the arrow/vertex configurations of the F-model and the 4-8/4/1 dimer model is shown in figure 13 for sublattice A. The correspondence on the B, C and D sublattices is affected by two considerations. First, the correspondence reverses the arrows on the B and D sublattices, thereby reversing the staggered field S on vertices w_5 and w_6. Second, the rotation of the locations of the low energy dimers on the squares shown in figure 2 translates to a quarter field Q that couples to the arrow configurations w_i, $i = 1, \ldots, 4$. The Q field points in the NW direction on the A sublattice, the NE direction on the B sublattice, the SE direction on the C sublattice and the SW direction on the D sublattice. The F-model vertices with polarization along

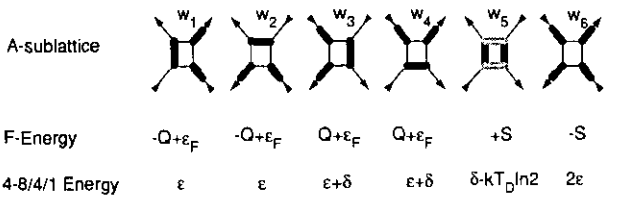

Figure 13. Correspondence between dimer configurations in the 4-8/4/1 model and arrow configurations in the F-model for the A-sublattice. The arrow configuration w_5 corresponds to two dimer configurations shown by black dimers and grey dimers, respectively.

(opposite) these directions have energy $\varepsilon_F - Q$ ($\varepsilon_F + Q$). The Q field contrasts with direct fields V and H which point in the same direction on all sublattices.

Figure 13 also shows the energies of the 4–8/4/1 dimer model, which is a free energy in the case of w_5 since this corresponds to two dimer configurations. The partition functions are related by

$$Z_F(S, Q; T_F) = (2wz^2)^{-4N} Z_{4\text{-}8/4/1}(z, w; T_D) \tag{23}$$

which effectively normalizes the ground states of the two models. Inclusion of the factor $(2wz^2)^{-1/2}$ results in the modified dimer activities $w_1 = w_2 = (2w)^{-1/2}$, $w_3 = w_4 = (w/2)^{1/2}$ and $w_5 = 1/w_6 = (2w/z^2)^{1/2}$. Equating Boltzmann factors for the F-model for $w_1 w_3$ yields

$$\exp(-2\varepsilon_F / kT_F) = \tfrac{1}{2} \tag{24}$$

which is just the equation that determines the only value of T_F for which the F-model may be solved as a dimer problem. Since T_F is fixed, it is convenient to absorb a factor of $1/kT_F$ into the F-model fields S and Q. Then, equating the Boltzmann factors for w_1/w_3 yields

$$2Q = \delta / kT_D = r/(kT_D/\varepsilon) \tag{25}$$

and equating the Boltzmann factor for w_6 vertices yields

$$2S = (\delta - 2\varepsilon)/kT_D - \ln 2. \tag{26}$$

Other useful correspondences include the direct polarization P and the staggered polarization P_S of the F-model,

$$P = \rho_x/2 \qquad P_S = -2 + (\rho_z/2). \tag{27}$$

Using the exact solution for the 4–8/4/1 dimer model in section 3 and the correspondences in (25) and (26), it is straightforward to obtain the phase diagram shown in figure 14 for the F-model in S and Q fields at the temperature T_F given by (24). This

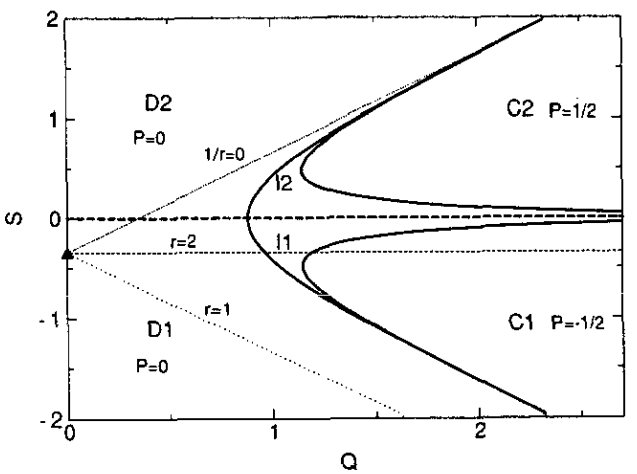

Figure 14. Q–S phase diagram for the F-model at one T_F. The solid lines are K-type transitions and the bold dashed line at $S = 0$ is the O-type line. The names of the corresponding phases in the 4-8/4/1 model are indicated and the direct polarization P is shown for those phases with constant ρ_x. Three thermal trajectories for the 4-8/4/1 dimer model are shown in light dotted lines with the solid triangle showing $T_D = \infty$.

phase diagram reveals the symmetries between the X1 and X2 phases, where X = C, I or D, in figure 1. Also, the O-line in figure 1 is the $S = 0$ line in figure 14. Unlike the K-type transitions involving walls, this is not a transparent quantity in the dimer models. Therefore, this correspondence adds insight into the behaviour of the 4-8/4/1 dimer model.

Along the $S = 0$ O-line the staggered susceptibility diverges, although the amplitude of the logarithmic singularity grows smaller with increasing Q. This result is not immediately obvious for the OK multicritical value Q_{OK} because the asymptotic form for det **M** changes to

$$\det \mathbf{M}(\theta, \phi, w, z) \sim (S^4 + \theta^2 + \phi^2)^2 + (S\phi)^2 \tag{28}$$

which is different from both the O-type form in (12) and the OK multicritical form in (14). However, a closely similar analysis to that in section 5 shows that the staggered susceptibility continues to diverge logarithmically with S.

It is interesting to contrast the S-Q phase diagram in figure 14 with the phase diagram for the F-model in an S field and a direct field. There are basically two distinct types of direct field that may be considered. In Baxter's (1970) notation V is a direct field pointing in the NW direction for all sublattices for the polarized vertices in figure 13. (The 4-8/2/1 dimer model discussed by Nagle and Yokoi (1987) corresponds to the F-model in a V field, as noted by Onody and Kurak (1988).) We will call the direct field D if it points in the N (vertical) direction in figure 13; in Baxter's notation this is $V = H$. Figure 15 shows both the S-V and S-D phase diagrams. As pointed out by Baxter (1970), the V field is special in that there is no perfectly ordered high field phase. However, the particular feature of interest in comparing with figure 14 is common to both types of direct field, namely, the O-type transition occurs only at the origin in figure 15. The application of any direct field removes the O-type transition and replaces it with K-type transitions.

In contrast to figure 15 the O-type transition in figure 14 persists for all non-zero values of the field Q and the K-type transitions are either prevented from crossing the Q-axis or do so with zero amplitude at the OK multicritical point. Another way to

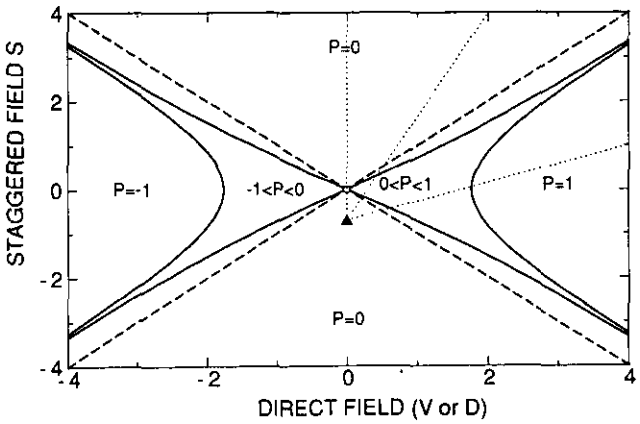

Figure 15. Phase diagram for the F-model at one temperature in staggered field S and direct field D (solid lines) and V (dashed lines) with values of direct polarization P indicated. Each dotted line corresponds to $0 < T_D < \infty$ for a fixed set of energies in a dimer model, such as the 4-8/2/1 model. The solid triangle shows $T_D = \infty$.

describe the phenomena is first to note that reversal of the staggered S field is associated with the O-type transition whereas K-type transitions seem to require either direct or quarter fields. In these terms the phase diagram in figure 15 suggests that the direct field dominates the staggered field whereas the phase diagram in figure 14 suggests that the staggered field dominates the quarter field. It may be of interest in future work to determine the phase behaviour when all three fields are applied.

Acknowledgments

We should like to thank M E Fisher for helpful discussion regarding OK multicritical scaling. One of us (CSOY) acknowledges the financial support by CNPq (Conselho de Desenvolvimento Cientifico e Tecnologico) and International Development Bank Project.

Appendix. Details of OK scaling form analysis

To determine the asymptotic behaviour of the free energy starting from (10) and (11), it is convenient to use polar coordinates for the integrations, first defining r and α from $r^2=\theta^2+\phi^2$ and $\phi=r\sin\alpha$ and then using $x=r^2$. Then (11) becomes

$$\det \mathbf{M}=(t_k t_o^2+x)^2+x(t_o\sin\alpha)^2. \tag{29}$$

Instead of working directly with (10) it is easier first to analyse the derivatives

$$u_i=\frac{\partial}{\partial t_i}f_s=\int_0^{x_c}\mathrm{d}x\int_0^{\pi/2}\mathrm{d}\alpha\,\frac{1}{\det \mathbf{M}}\,\frac{\partial}{\partial t_i}\det \mathbf{M} \tag{30}$$

where i is o or k and

$$\frac{\partial}{\partial t_k}\det \mathbf{M}=2t_o^2(t_k t_o^2+x)\qquad \frac{\partial}{\partial t_o}\det \mathbf{M}=2[\det \mathbf{M}+(t_k^2t_o^4-x^2)]/t_o. \tag{31}$$

Using (31) the α integration was carried out in (30). It involves

$$\int_0^{\pi/2}\mathrm{d}\alpha/\det \mathbf{M}=\pi/2X^{1/2}Y \tag{32}$$

where

$$Y=|x+t_k t_o^2|\qquad\text{and}\qquad X=x^2+t_o^2(2t_k+1)x+t_k^2t_o^4$$

with the results

$$u_k=\pi t_o^2\int_0^{x_c}\operatorname{sign}(t_k t_o^2+x)X^{-1/2}\,\mathrm{d}x \tag{33}$$

and

$$u_o=(\pi/t_o)\int_0^{x_c}[1+\operatorname{sign}(t_k t_o^2+x)(t_k t_o^2-x)X^{-1/2}]\,\mathrm{d}x. \tag{34}$$

Then, the x integration was carried out in (33) and (34), using the following identities,

$$t_k t_o^2-x=[t_o^2(1+4t_k)-(\mathrm{d}X/\mathrm{d}x)]/2 \tag{35}$$

and

$$\int X^{-1/2}\,dx = \ln[2X^{1/2}+2x+t_o^2(2t_k+1)] \equiv F(x). \tag{36}$$

For $t_k > 0$ this gives

$$u_k = \pi t_o^2[F(x_\varepsilon) - F(0)] \tag{37}$$

and

$$u_o = (1+4t_k)u_k/2t_o + \pi(x_\varepsilon - X(x_\varepsilon)^{1/2} + X(0)^{1/2})/t_o. \tag{38}$$

For $t_k < 0$ the results are

$$u_k = \pi t_o^2[F(x_\varepsilon) + F(0) - 2F(|t_k|t_o^2)] \tag{39}$$

and

$$u_o = (1+4t_k)u_k/2t_o + \pi[x_\varepsilon - X(x_\varepsilon)^{1/2} - X(0)^{1/2} + 2X(|t_k|t_o^2)^{1/2}]/t_o. \tag{40}$$

The contributions from $F(x_\varepsilon)$, $X(x_\varepsilon)^{1/2}$ and $X(0)^{1/2} = |t_k t_o^2|$ are regular and will be ignored. The remaining singular contributions are, for $t_k > 0$,

$$\begin{aligned} u_k &= -2\pi t_o^2 \ln|t_o| \\ u_o &= -\pi t_o(1+4t_k)\ln|t_o| \end{aligned} \tag{41}$$

and for $t_k < 0$, are

$$\begin{aligned} u_k &= -2\pi t_o^2 \ln|t_o| - \pi t_o^2 \sum_{n=1}^{\infty} 2^{2n}|t_k|^{(2n-1)/2}/(2n-1) \\ u_o &= -\pi t_o(1+4t_k)\ln|t_o| + \pi t_o \sum_{n=1}^{\infty} 2^{2n+3}|t_k|^{(2n+1)/2}/(4n^2-1). \end{aligned} \tag{42}$$

The above results may then be integrated to obtain the results for the leading singular parts of f_s given in (15) and (16) in the text.

References

Andrews G E, Baxter R J and Forrester P J 1984 *J. Stat. Phys.* **35** 193

Baxter R J 1970 *Phys. Rev.* B **1** 2199

Baxter R J 1982 *Exactly Solved Models in Statistical Mechanics* (London: Academic)

Bhattacharjee S M 1984 *Phys. Rev. Lett.* **53** 1161

Fisher M E 1983 *Critical Phenomena (Lecture Notes in Physics)* ed F J W Hahne (Berlin: Springer) ch 1

Kasteleyn P W 1963 *J. Math. Phys.* **4** 287

McCoy B M and Wu T T 1973 *The Two-Dimensional Ising Model* (Cambridge, MA: Harvard University Press)

Montroll E W 1964 *Applied Combinatorial Mathematics* ed E F Beckenback (New York: Wiley) ch 4

Nienhuis B, Hilhorst H J and Blote H W J 1984 *J. Phys. A: Math. Gen.* **17** 3559

Nagle J F, Yokoi C S O and Bhattacharjee S M 1989 Dimer models on anisotropic lattices *Phase Transitions and Critical Phenomena* ed C Domb and J L Lebowitz (New York: Academic) ch 2

Nagle J F and Yokoi C S O 1987 *Phys. Rev.* B **35** 5307

Onody R N and Kurak V 1988 *Phys. Rev.* B **38** 5061

Onsager L 1944 *Phys. Rev.* **65** 117

Pokrovsky V L and Talapov A L 1979 *Phys. Rev. Lett.* **42** 65

Wu F Y and Lin K Y 1975 *Phys. Rev.* B **12** 419

Yokoi C S O, Nagle J F and Salinas S R 1986 *J. Stat. Phys.* **44** 729